"Supra" Crystal: Control of the Ordering of Self-Organization of Cobalt Nanocrystals at the Mesoscopic Scale

Isabelle Lisiecki,[†] Pierre-Antoine Albouy,[‡] and Marie-Paule Pileni*,[†]

Laboratoire LM2N, UMR CNRS 7070, Université P. et M. Curie, Bât. F, 4 Place Jussieu, 75005 Paris, France, and Laboratoire de Physique des Solides, UMR 8502, Université Paris-Sud, Bât. 510, 91405 Orsay, France

Received: June 17, 2004

Cobalt nanocrystals with very low size distribution self-assemble to produce well-grown face-centered cubic (fcc) "supra" crystals. By adjusting the substrate temperature during the solvent evaporation process, structural ordering is controlled. Hence, it is possible to obtain either a long-range arrangement of the magnetic nanocrystals or a short-range ordering. The film morphology can be improved in terms of homogeneity and crack density by lowering the evaporation rate of the solvent. The ordering of the nanocrystals into a "supra" crystal is accompanied by a slight change of the magnetic properties.

I. Introduction

In the past few years, several groups have concentrated their efforts on producing self-organized magnetic nanocrystals in a 2D superlattice. When magnetic nanocrystals are deposited on a surface, collective properties due to long-range dipolar interactions are observed.[1−11] No change in the magnetic response is obtained when the nanocrystals are locally ordered in 2D.[12] However, drastic changes are observed when the nanocrystals are aligned along a given direction.[12,13] To our knowledge, most of the studies related to collective magnetic properties are performed when the nanocrystals are organized in 2D superlattices.[1−5,7,8,10−12] In 3D mesoscopic structures built up with maghemite particles, which are not organized in well-defined superlattices, the influence of the film structure on the collective properties has been clearly demonstrated.[6,9,13] In all these cases, the influence of long-range ordering of the nanocrystals has been studied. Recently, we have shown that cobalt nanocrystals self-organize into long-range scale in fcc supra-crystals.[14]

In the present paper, we show that the adjustment of the experimental conditions of the deposition process leads to either disordered or highly ordered 3D assemblies. These are built with the same nanocrystal population (i.e., the same size and the same size distribution). Magnetic properties are compared for both disordered and ordered assemblies. The effect of the evaporation rate on the cobalt film morphology is also presented.

II. Experimental Section

II. A. Products. All materials were used without further purification. Cobalt acetate, lauric acid, and sodium borohydride are from Aldrich; isooctane and hexane are from Fluka, and sodium di(ethylhexyl) sulfosuccinate (Na(AOT)) is from Sigma. The synthesis of cobalt(II) bis(2-ethylhexyl)sulfosuccinate, ($Co(AOT)_2$) has been described previously.[15]

II. B. Equipment. Scanning electron microscopy was performed with a JMS-5510LV instrument. X-ray diffraction experiments were performed with a rotating anode generator operated with a small-size focus (copper anode; focus size 0.2 mm × 0.2 mm; 50 kV, 30 mA). The optics consisted of a parabolic multilayer graded mirror followed by a bent, nickel-coated mirror at right angles providing a parallel monochromatic beam. The sample was mounted on a rotation stage, and the diffraction patterns were recorded on photostimulable imaging plates. Vacuum pipes are inserted between the sample and the imaging plate to reduce air scattering.

The magnetic measurements were made with a commercial SQUID magnetometer (Cryogenic S600).

The partial pressure of the hexane vapor was measured with a system based on the wet and dry bulbs system: The temperature difference between a hexane-soaked paper wick and the atmosphere was obtained with a differential thermocouple.

II. C. Synthesis of Cobalt Nanocrystals. Synthesis of cobalt nanocrystals coated with lauric acid is described in ref 16. Reverse micelles of 5×10^{-2} M $Co(AOT)_2$ form an isotropic phase. The amount of water added in solution is fixed to reach a water concentration defined as $w = [H_2O]/[AOT] = 32$. Sodium borohydride, $NaBH_4$, added to the micellar solution reduces the cobalt ions. The sodium borohydride content is defined as $R = [NaBH_4]/[Co(AOT)_2] = 6$. Immediately after $NaBH_4$ addition, the micellar solution color turns from pink to black, indicating the formation of colloidal cobalt particles. The nanocrystals are coated and then extracted from the surfactant. The coating process is obtained as follows: In the solution containing nanocrystals, surfactants, water, and isooctane, 0.2 M lauric acid, $C_{12}H_{25}COOH$, is added, inducing a chemical bond between O of lauric acid and Co atoms located at the interface. The coated cobalt nanocrystals are then washed and centrifuged several times with ethanol to remove all of the AOT surfactant, and the obtained black powder is dispersed in hexane. To eliminate the largest particle size formed, the solution is centrifuged, and only the upper phase containing the smallest particle sizes is collected. At the end of the synthesis, 7.2 nm-cobalt nanocrystals coated with lauric acid and characterized as a 12% size distribution are produced.

II. D. Sample Preparation. After synthesis, the concentration of the nanocrystals dispersed in hexane is fixed at 5.5×10^{-7} M. HOPG pieces (5 mm × 5 mm) are horizontally immersed in 200 μL of this highly concentrated nanocrystal solution. During solvent evaporation, the substrate temperature is controlled by a Peltier cooling stage. Nitrogen, whose flow can be adjusted, is used to prevent cobalt oxidation; the evaporation

[†] Université P. et M. Curie.
[‡] Université Paris-Sud.

10.1021/jp0473725 CCC: $27.50
Published on Web 12/04/2004

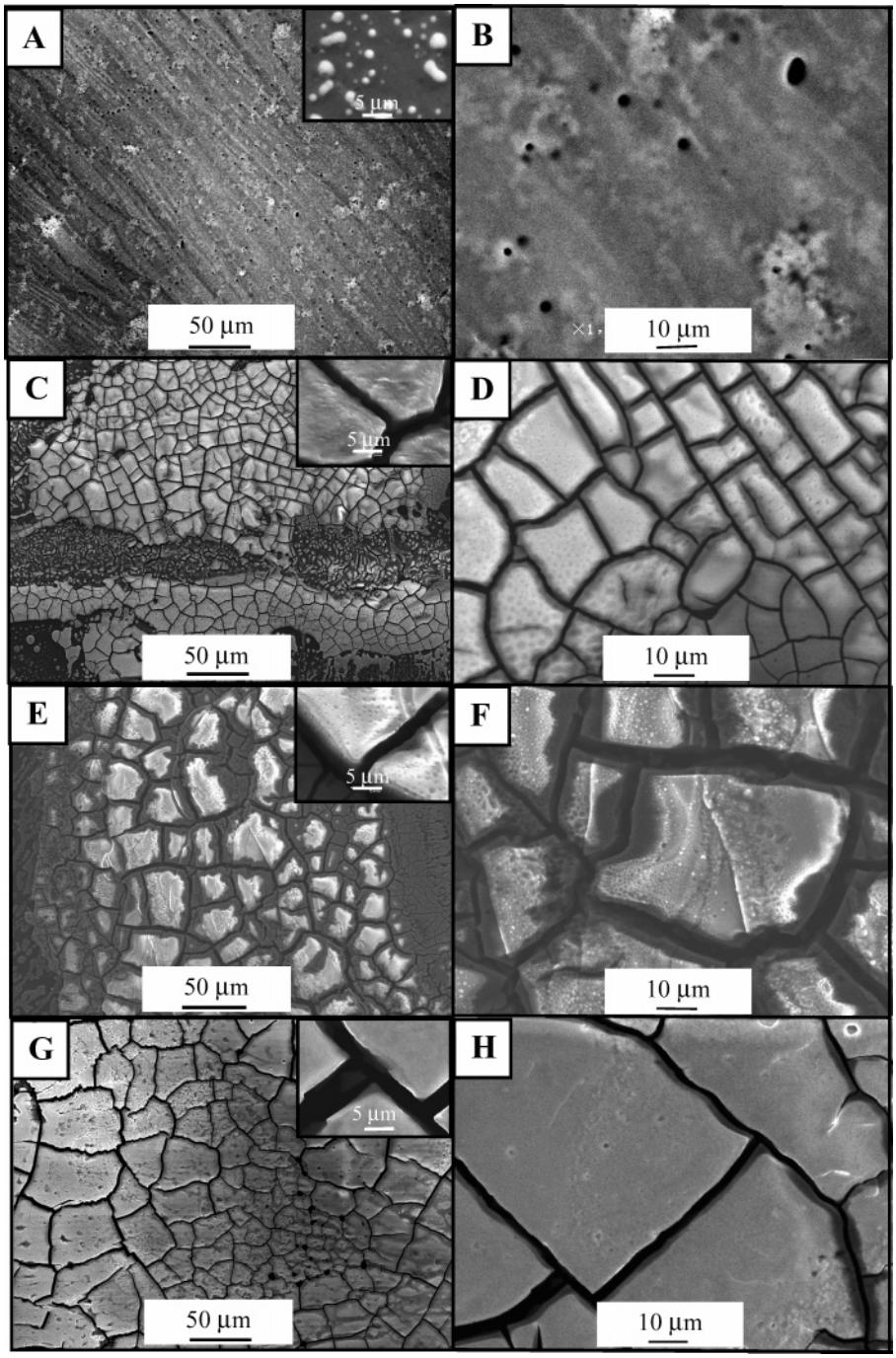

Figure 1. SEM patterns obtained from HOPG substrate immersed in 200 μL of a highly concentrated cobalt colloidal solution, evaporated under a nitrogen atmosphere close to a solvent saturation equal to 40%. The different substrate temperatures are (A, B) $T = 10$ °C, (C, D) $T = 25$ °C, (E, F) $T = 35$ °C, (G, H) $T = 45$ °C. Inserts of figures A, C, E, F: Corresponding high-magnification SEM patterns.

rate is presently characterized by the hexane partial pressure in the evaporation cell.

III. Results and Discussion

III. A. Effect of Temperature. In the text that follows, the hexane partial pressure is kept at ca. 40% of the saturation value (regardless of the solution temperature, the atmosphere temperature remains close to room temperature). By changing the substrate temperature, we observed two specific behaviors:

In the temperature range $5 < T < 12$ °C, the deposition gives rise to the formation of a thin film coexisting with aggregates. Figure 1A,B shows a nonhomogeneous cobalt film observed at 10 °C. Holes and small aggregates are observed (Figure 1B). The insert Figure in 1A shows the formation of isolated aggregates characterized by a rather large inhomogeneity in shape and size, and the walls are not well-defined. The X-ray diffraction pattern (insert Figure 2A) reveals a broad, diffuse ring attributed to an amorphous material. This is confirmed by the $\Theta-2\,\Theta$ diffractogram (Figure 2A) showing a low-intensity peak characterized by a half-width at half-maximum $\delta q_{1/2} = 0.19$ nm^{-1}, markedly larger than the resolution equal to 0.03 nm^{-1} (Table 1). The corresponding correlation length is crudely estimated by application of the Scherrer formula $0.888.\pi/\delta q_{1/2}$ (i.e., 15 nm). The peak-to-ring intensity ratio R_{int} can be used to characterize the degree of preferential orientation; it is presently rather low (i.e., 1.6).

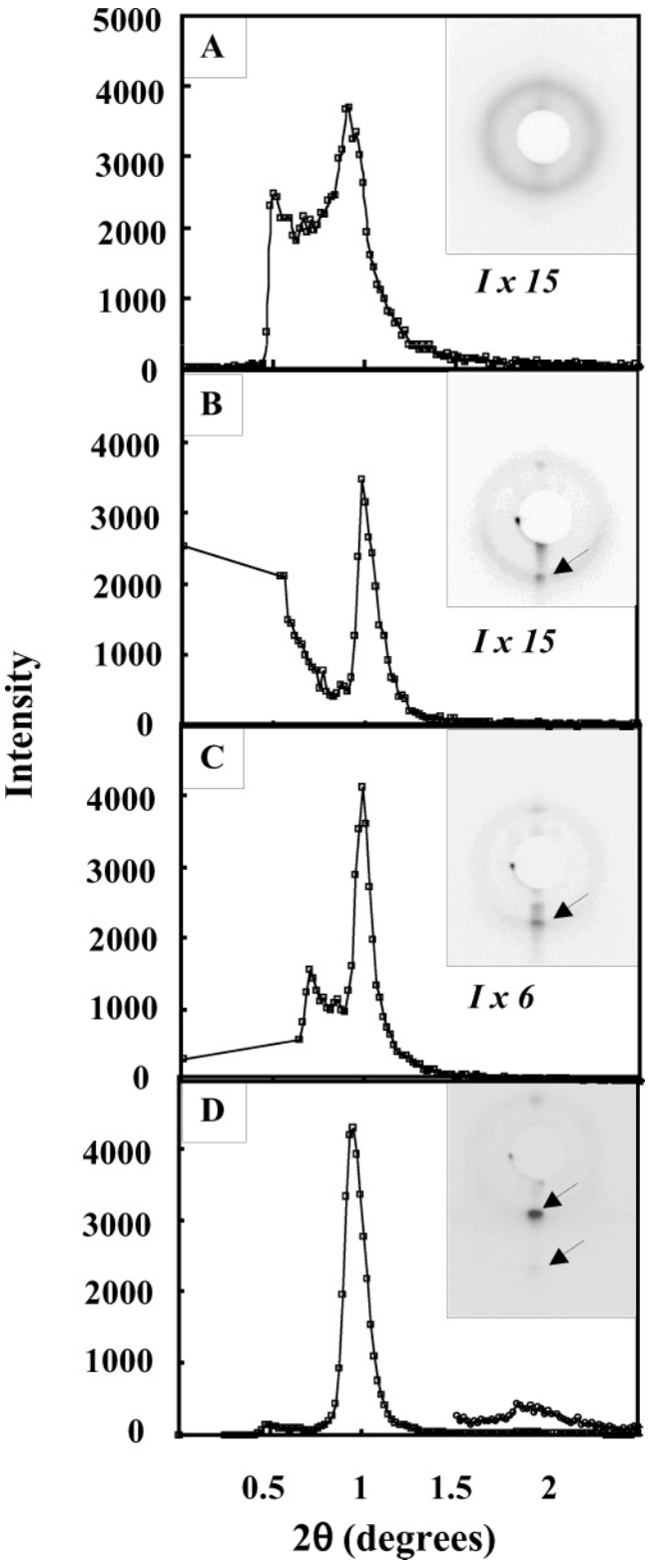

Figure 2. Diffractograms of cobalt films shown in Figure 1: (A) $T = 10$ °C, (B) $T = 25$ °C, (C) $T = 35$ °C, (D) $T = 45$ °C. Insert: Diffraction patterns.

In the temperature range $18 < T < 45$ °C, the film morphology drastically changes (Figure 1C−H). Isolated domains that look like pavements are observed. It has to be noted that, regardless of the substrate temperature, the substrate coverage by nanocrystals is not homogeneous. In fact, most of the nanocrystals are deposited at the border of the substrate. Upon increasing the substrate temperature, the pavement area increases. For temperatures equal to 25 , 35, and 45 °C, the average domain areas are 400 , 1000, and 2500 μm^2, respectively. Various SEM image magnifications (inserts of Figure 1C,E,G and Figure 1D,F,H) show that the surfaces of the domains appear fairly smooth. In addition, regardless of the substrate temperature, the edges are well-defined. The average distance between pavements varies from 2 to 5 μm, and their heights reach 5 μm. The X-ray diffraction patterns (inserts in Figure 2B− D) clearly show the high ordering of the nanocrystals.

TABLE 1: Various Parameters Extracted from the Diffraction Patterns and the Corresponding Diffractograms[a]

substrate temperature	12 °C	25 °C	35 °C	45 °C
inner ring distance (nm)	9.60	8.80	8.80	8.70
$\delta q_{1/2}$ (nm^{-1})	0.19	0.050	0.035	0.034
$R_{int} = I_{ref}/I_{halo}$	1.6	11	87	674
$D_{center-center}$ (nm)	11.75	10.80	10.80	10.65
$D_{interpart}$ (nm)	4.55	3.60	3.60	3.45

[a] $\delta q_{1/2}$: half-width at half-maximum. R_{int}: the reflection intensity to the halo intensity ratio. $D_{center-center}$: center-to-center nanocrystal distance. $D_{interpart}$: border-to-border nanocrystal distance.

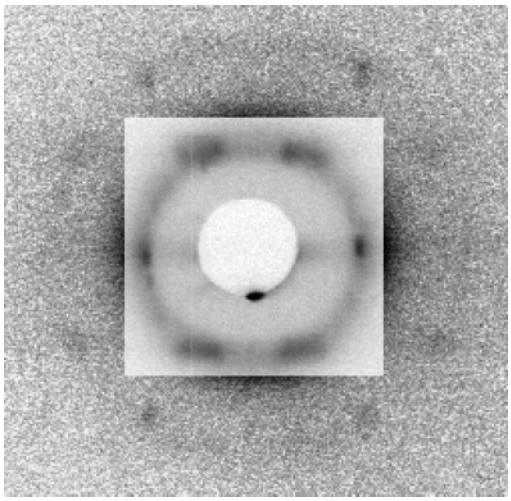

Figure 3. X-ray diffraction pattern obtained in a nearly grazing incidence geometry. Tilt angle of substrate surface with respect to the incoming beam is 10°. The intensity is reduced by a factor of 20 in the central inset. The solvent evaporation is made at a substrate temperature equal to 45 °C.

At 25 °C, the X-ray diffraction pattern displays a weak ring with a strong reinforcement normal to the substrate, indicating a marked preferential orientation of the domains (insert in Figure 2B). The reflection width (Figure 2B) is nearly resolution-limited (i.e., 0.05 nm^{-1}, indicating long-range ordering out of the plane of the nanocrystals). The peak-to-ring intensity ratio, R_{int}, is relatively high (i.e., 11) compared to the sample obtained at 10 °C (Table 1). The corresponding periodicity deduced from the position of the peak is found equal to 8.80 nm.

By increasing the temperature from 25 to 35 and 45 °C, the peak width $\delta q_{1/2}$ decreases from 0.05 to 0.035 and 0.034 nm^{-1}, respectively, while the ratio R_{int} drastically increases from 11 to 87 and 674, respectively (Inserts in Figure 2B−D and Table 1). At 45 °C, a second-order reflection appears (Insert in Figure 2D). This behavior clearly indicates an increase in both size and ordering of the "supra" crystals. By tilting the sample, the amount of intercepted beam may be enhanced so that numerous additional diffraction spots become visible. By comparing the experimental spot coordinates obtained at 45 °C (Figure 3) and the theoretical values of various structures, it can be concluded to be an fcc structure, as observed previously for a "supra" crystal made at 25 °C with another evaporation process.[13]

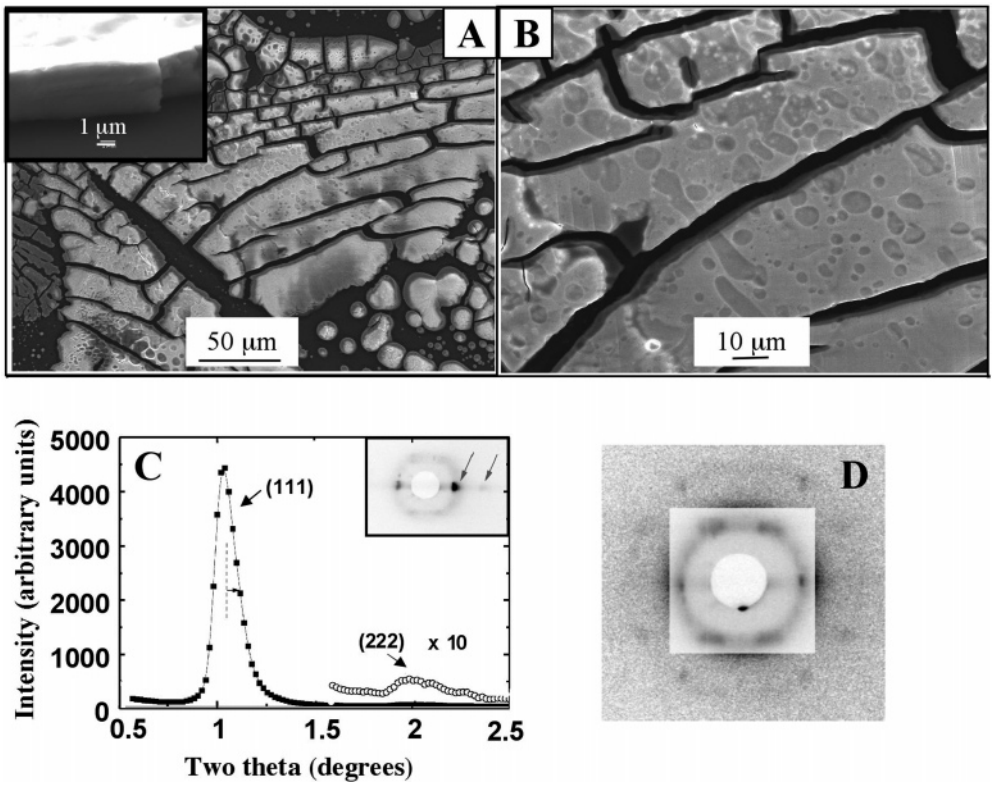

Figure 4. (A) SEM patterns showing Co "supra" crystals obtained under a dry nitrogen atmosphere. (C) The $\Theta-2\Theta$ diffractogram and, in inset, the corresponding X-ray diffraction pattern. (D) The X-ray diffraction pattern (tilt angle of substrate surface with respect to the incoming beam is 10°).

Diffraction patterns obtained at 25 and 35 °C are similar to those obtained at 45 °C and allow us to conclude that, for the three ordered samples, cobalt domains consisting of fcc crystals are formed, with the [111] axis normal to the substrate and an in-plane random orientation. The stacking parameter that corresponds to the ring distance (d_{111} distance) does not exhibit any significant dependence upon deposition temperature (Table 1). As a matter of fact, for substrate temperatures equal to 25, 35, and 45 °C, the stacking periodicities are 8.80, 8.80, and 8.70 nm, respectively. The stacking periodicity for the fcc structure is $D_{\text{center-center}}\sqrt{2/3}$, where $D_{\text{center-center}}$ is the center-to-center distance between neighboring nanocrystals. The corresponding $D_{\text{center-center}}$ values are then 10.80, 10.80, and 10.65 nm, respectively. By taking into account these three values related to the three ordered systems, let us consider the average center-to-center distance between neighboring nanocrystals (i.e., 10.75 nm). Assuming a core diameter of 7.2 nm, we find the resulting interparticle distance to be 3.55 nm. This distance is quite similar to twice the all-trans length of lauric acid (1.78 nm $\times$ 2) and clearly confirms the following:

(i) the absence of interdigitations between the lauric acid chains

(ii) the compact packing of the so-coated cobalt nanocrystals.

If we assume that the local packing in the amorphous assembly resembles the one found in the cubic "supra" crystal, the values of $D_{\text{center-center}} = 11.75$ nm and $D_{\text{interpart}} = 4.55$ nm are found. As expected, the packing of Co nanocrystals is less compact (the difference is 1 nm) in the amorphous phase than in the supra-crystal.

The dependence of the structural organization upon the deposition temperature may be related to results obtained by Courty et al.[17] from which the change in the ordering is obtained by controlling the substrate temperature. The parameters involved in this structural change include the diffusion coefficient of the nanocrystals and their solubility in hexane. It can be speculated that a temperature that is too low leads to a rapid aggregation of particles that cannot correctly organize. It is also possible that the coating fluidity plays a role in the reorganization of precipitates. Indeed, it is known that CH_2 units become more and more mobile as the temperature becomes closer to 40 − 50 °C.

From these data, it is concluded that, by changing the substrate temperature, it is possible to produce either well-defined "supra" crystals characterized by an fcc structure or disordered assemblies of nanocrystals. Furthermore, the packing of magnetic nanocrystals is more compact, with 3.55 nm as the average distance between nanocrystals, when they are organized in cubic structures, than that obtained with disordered aggregates (average distance of 4.55 nm).

III. B. Effect of Evaporation Rate. The role of the evaporation rate may be addressed at this point. With the substrate temperature fixed at 25 °C, the film morphologies and structures are compared when the nitrogen flow is not hexane-saturated at all and, conversely, when the hexane partial pressure is kept at ca. 40% (sample described already) and ca. 100% of the saturation value. For simplicity, let us consider the various samples as **I**, **II**, and **III**, respectively. Isolated pavements, with a rather large size distribution, are produced with samples **I** and **II** (Figures 4A,B and 1C,D). However, with sample **I**, the pavements are larger than those obtained with sample **II** (Figure 4A). When the nitrogen flow is almost 100% saturated by hexane, drastic changes on the SEM image are observed (Figure 5):

(i) The absence of pavements.

(ii) The surface of the film of nanocrystals is not smooth anymore and presents many terraces. Regardless of the sample, the deposition of cobalt nanocrystals is never homogeneous. It is thicker at the border than in the center of the HOPG substrate.

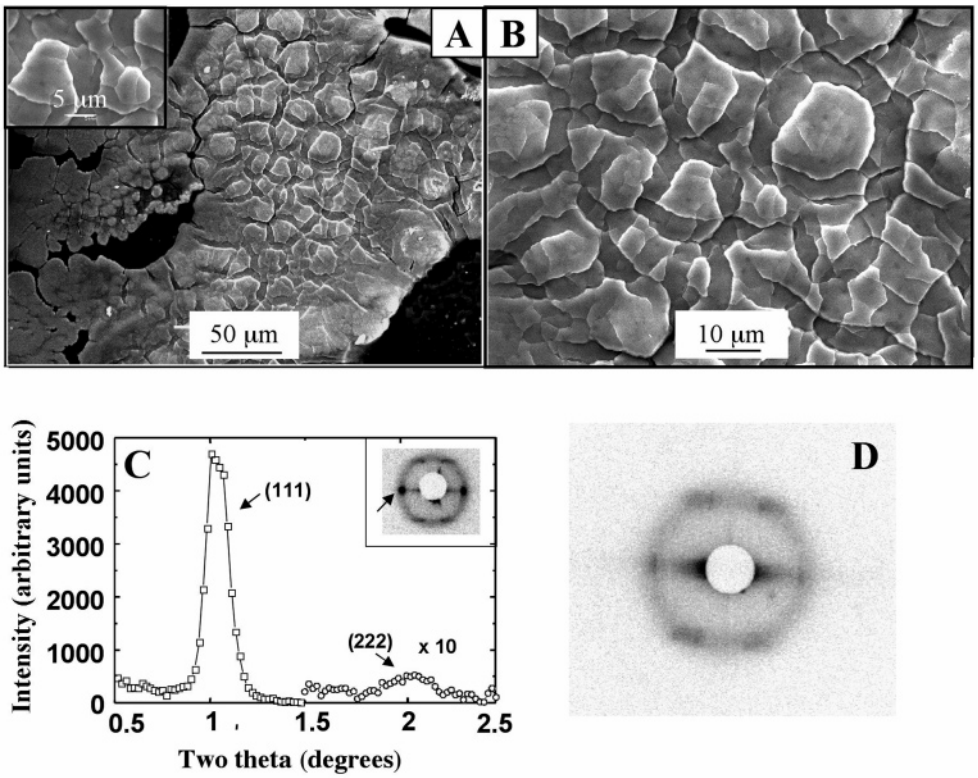

Figure 5. (A) SEM patterns showing Co "supra" crystals obtained under a nitrogen atmosphere close to a solvent saturation equal to 100%. (C) The Θ−2 Θ diffractogram and, in insert, the corresponding X-ray diffraction pattern. (D) The X-ray diffraction pattern (tilt angle of substrate surface with respect to the incoming beam is 10°).

Regardless of the evaporation rate, the X-ray diffraction data clearly indicate the formation of fcc artificial solids characterized by long-range ordering out of the plane. Indeed, the X-ray diffraction patterns of samples **I**, **II**, and **III** always show a weak ring and a strong reinforcement normal to the substrate, indicating a marked preferential orientation of the domains (inserts in Figures 4C, 2B, and 5C). By tilting the samples, the reflections of a cubic structure are obtained (Figures 4D, 3, and 5D). It has to be noted that the absence of the outer reflections for sample **III** (Figure 5D) is only due to the fact that the tilt is not optimal. Nevertheless, the inner reflections are quite sufficient to conclude that it is a cubic structure. From the Q−2Q diffractograms, the reflection widths (Figures 4C, 2B, and 5C) are found equal to 0.044, 0.050, and 0.050 nm^{-1}, respectively, and the reflection intensity to the halo intensity ratios are 20.5, 11, and 15.5, respectively. The corresponding periodicities are 8.54, 8.80, and 8.64 nm, respectively. The absence of a second-order (111) reflection for sample **II** has to be noted. This fact could be related to the size of the crystallographic domain, which is smaller for sample **II** as compared to samples **I** and **III**. As a matter of fact, the structural characteristics of these three artificial solids are fairly similar and clearly indicate that, regardless of the evaporation conditions, we form well-grown fcc "supra" crystals. The change in the supra-crystal morphology with hexane saturation of the nitrogen flow (i.e., the formation of either smooth pavements or terraces has to be related to the change in the evaporation rate). Indeed, the cracks are more pronounced when the hexane saturation is less than 100% (i.e., when the rate evaporation is high). In fact, the formation of cracks results from the high surface tension arising during solvent evaporation that is too rapid. In the present experiments, all of the samples are characterized by a non-homogeneous film. It is always thicker at the border than in the center of the HOPG substrate. Partly related to this fact and also the nonhomogeneous HOPG substrate's flatness and hydrophobicity, various nucleation centers of the "supra" crystals form, explaining the various orientations of the "supra" crystal domains (i.e., the in-plane disorder of the film). Hence, we have been able to produce either magnetic cubic "supra"-crystals, characterized by various film morphologies, or disordered films. The cobalt nanocrystal unit used to build these various assemblies is a constant (i.e., characterized by an average size of 7.2 nm) with a size distribution of 12%.

III. C. Magnetic Investigation. At this point of the study, we want to know if this long-range ordering plays a role in the magnetic properties. Because the three various samples produced at 25 °C are similar and characterized by the same fcc structure, we will concentrate our magnetic study on aggregates forming amorphous assemblies as shown in Figure 1A,B and "supra" crystals (Figure 1C,D). The magnetization curves are recorded at 3 K, and the applied magnetic field is parallel to the HOPG substrate. For "supra" crystals, the saturation magnetization is reached at 0.3 T, whereas with the amorphous aggregate, it is approximately 1.5 T (Figure 6). In both cases, the saturation magnetization (120 emu/g) and coercivity (0.07 T) are similar to data previously published for a monolayer of cobalt nanocrystals disordered or locally ordered.[18] As already observed and expected for nanocrystals, the saturation magnetization is lower that that of the bulk phase (162 emu/g). The zero-field cooled and field cooled (ZFC/FC) curves, recorded with a 75 Oe field (insert in Figure 6) shows a lower blocking temperature for amorphous aggregates (around 95 K) compared to that obtained for the "supra" crystal (around 115 K). To explain such differences, let us take into account the structural results described already. Table 1 shows a change of 1 nm of the average distance between nanocrystals with their organization. This induces a change in

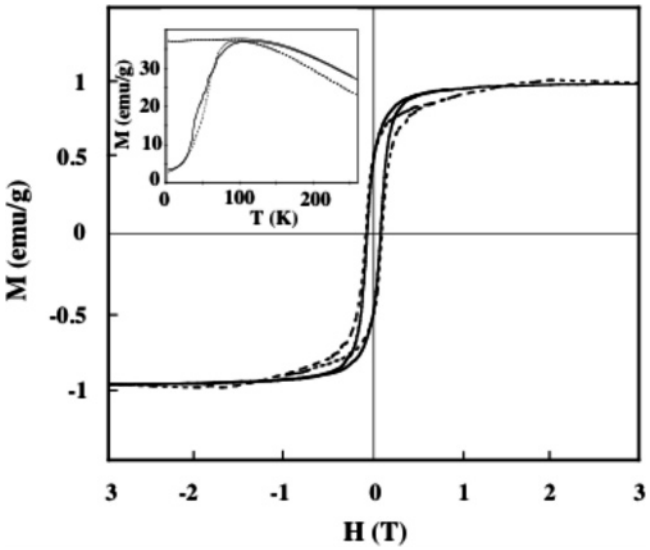

Figure 6. Hysteresis magnetization loops of 3D assembly of 7.2-nm Co nanocrystals, obtained at 3 K. In inset, the ZFC/FC curve. Amorphous assembly (dotted line); supra-crystal (full line).

the coupling constant, α_d. Assuming dipolar interactions modeled by Stoner−Wohlfarth for magnetic particles,[19,20] it has been calculated as

$$\alpha_d = \frac{\pi}{12}\frac{M_s^2}{K}(D/d)^3$$

where K, M_s, D, and d are the anisotropy constant ($K = 1.5 \times 10^6$ erg/cm^3), the saturation magnetization ($M_s = 120$ emu/g), the magnetic nanocrystal diameter ($D = 7.2$ nm), and the center-to-center distance of the cobalt nanocrystals. This distance is 11.75 and 10.75 nm for the amorphous and highly ordered aggregates, respectively. According to the decreasing of this distance, the coupling constant evolves from 0.025 to 0.030. This change in the average distance between nanocrystals explains the evolution of the hysteresis loop through the saturation magnetization reached at relatively low applied field and that of the blocking temperature. However, an intrinsic change in the magnetic properties, caused by the high ordering of the cobalt nanocrystals in "supra" crystals at the mesoscopic scale, cannot be excluded. To verify this hypothesis, we have to be able to build ordered and disordered assemblies characterized by the same nanocrystal diameters, as has been described in this paper, and also by the same distance between particles. This end could be achieved by tuning the length of the coating. That will be our next challenge. On the other hand, SQUID measurement gives rise to an average response all over the sample (i.e., all over the numerous supra-crystals characterized by an in-plane disorder). Local investigations are needed to give a final answer.

IV. Conclusion

In this paper, we show that temperature is a key parameter for controlling the ordering of films of cobalt nanocrystals. At low substrate temperature, ($5 < T < 12$ °C), an amorphous, continuous film is observed. At higher substrate temperature, ($18 < T < 45$ °C), the formation of a film presenting many cracks is favored. Such a film can be described as the juxtaposition of various fcc "supra" crystals whose average size and orientation improve with increasing temperature. By adjusting the partial vapor pressure of the solvent during evaporation (at room temperature), it is possible to obtain crack-free homogeneous films with a crystalline organization (high saturation degree). Magnetic studies show that the degree of "supra" organization of the Co nanocrystals has a slight influence on the magnetic properties of the film that could be explained in terms of dipolar interactions, and new data are needed to be able to exclude any intrinsic properties due to the high organization of nanocrystals.

Acknowledgment. We are grateful to Dr. O. Anitoff for his help with the temperature control apparatus. Thanks are due to Dr. J. Hamman, Dr. E. Vincent, and Dr. G. Lebras from CEA/Saclay/DRECAM/SPEC for experimental help in magnetization experiments. Thanks are also due to Dr. A. Ngo for providing SEM images.

References and Notes

(1) Petit, C.; Taleb, A.; Pileni, M. P. *J. Phys. Chem. B* **1999**, *103*, 1805.
(2) Petit, C.; Taleb, A.; Pileni, M. P. *Adv. Mater. (Weinheim, Ger.)* **1998**, *10*, 259.
(3) Murray, C. B.; Sun, S.; Gaschler, W.; Doyle, H.; Betley, T. A.; Kagan, C. R. *IBM J. Res. Dev.* **2001**, *45*, 47.
(4) Sun, S.; Murray, C. B.; Weller, D.; Folks, L.; Moser, A. *Science* **2000**, *287*, 1989.
(5) Russier, V.; Petit, C.; Legrand, J.; Pileni, M. P. *Phys. Rev. B* **2000**, *62*, 3910.
(6) Ngo, T.; Pileni, M. P. *Adv. Mater. (Weinheim, Ger.)* **2000**, *12*, 276.
(7) Black, C. T.; Murray, C. B.; Sandstrom, R. L.; Sun, S. *Science* **2000**, *290*, 1131.
(8) Russier, V. *J. Appl. Phys.* **2001**, *89*, 1287.
(9) Ngo, T.; Pileni, M. P. *J. Phys. Chem.* **2001**, *105*, 53.
(10) Legrand, J.; Petit, C.; Pileni, M. P. *J. Phys. Chem. B* **2001**, *105*, 5643.
(11) Ngo, T.; Pileni, M. P. *J. Appl. Phys.* **2002**, *92*, 4649.
(12) Petit, C.; Russier, V.; Pileni, M. P. *J. Appl. Phys.* **2003**, *107*, 10333.
(13) Lalatone, Y.; Motte, L.; Russier, V.; Ngo, A. T.; Bonville, P.; Pileni, M. P. *J. Phys. Chem. B* **2004**, *108*, 1848.
(14) Lisiecki, I.; Albouy, P. A.; Pileni, M. P. *Adv. Mater.* **2003**, *15*, 712.
(15) Petit, C.; Lixon, P.; Pileni, M. P. *Langmuir* **1991**, *7*, 2026.
(16) Lisiecki, I.; Pileni, M. P. *Langmuir* **2003**, *19*, 9486.
(17) Courty, A.; Fermon, C.; Pileni, M. P. *Adv. Mater. (Weinheim, Ger.)* **2001**, *13*, 254.
(18) Legrand, J.; Petit, C.; Bazin, D.; Pileni, M. P. *Appl. Surf. Sci.* **2000**, *164*, 186.
(19) Stoner, C.; E. Wohlfarth, P. *Philos. Trans. R. Soc. London, Ser. A* **1948**, *240*, 599, reprinted in *IEEE Trans. Magn.* **1991**, *27*, 3475.
(20) Pfeiffer, H. *Phys. Status Solidi A* **1990**, *122*, 377.